Organo-Soluble Polyimde (ODA–BSAA)/Montmorillonite Nanocomposite Materials Prepared by Solution Dispersion Technique

Jui-Ming Yeh,[1] Chi-Fa Hsieh,[1] Jenn-Huey Jaw,[1] Tai-Hung Kuo,[1] Hsi-Ya Huang,[1] Ching-Lung Lin,[2] Min-Yu Hsu[2]

[1] *Department of Chemistry and Center for Nanotechnology at CYCU, Chung-Yuan Christian University, Chung Li 32023, Taiwan, Republic of China*
[2] *Institute of Organic and Polymeric Materials, National Taipei University of Technology, Taipei 100, Taiwan, Republic of China*

Received 2 December 2003; accepted 9 July 2004
DOI 10.1002/app.21317
Published online in Wiley InterScience (www.interscience.wiley.com).

ABSTRACT: A series of polymer–clay nanocomposite materials, consisting of organo-soluble polyimide (ODA-BSAA) matrix and dispersed nanolayers of inorganic montmorillonite clay, were successfully prepared by solution dispersion technique and subsequently characterized by FTIR, powder X-ray diffraction patterns, transmission electron microscopy, and atomic force microscopy. Effects of the materials composition on the corrosion protection performance, gas barrier, and optical properties, in the form of both coating and film, were also studied by electrochemical corrosion measurements (e.g., corrosion potential, polarization resistance, corrosion current, impedance spectroscopy), gas permeability analysis, and UV–visible transmission spectroscopy, respectively. © 2005 Wiley Periodicals, Inc. J Appl Polym Sci 95: 1082–1090, 2005

Key words: polyimides; clay; nanocomposites; corrosion; coatings

INTRODUCTION

Recently, research topics associated with well-dispersed clay platelets (e.g., intercalation and/or exfoliation structures) in various polymer matrices, to prepare polymer–clay nanocomposite (PCN) materials with effectively enhanced chemical and/or physical properties, have evoked increasing attention because PCNs exhibit great potential for a wide range of commercial applications. Many polymer systems such as thermoplastic polymers [e.g., poly(methyl methacrylate),[1,11] polystyrene,[2] polyacrylonitrile,[3] and polyvinyl alcohol[4]], conducting polymers (e.g., polyaniline,[5] polythiophene,[6] and polypyrrole[7]), and thermosetting polymers (e.g., polyamide,[8] epoxy resin,[9] and nylon[10]) have been used to blend with clay platelets by different methods such as *in situ* polymerization,[1,5,7,11] solution dispersion,[4,12] and melt intercalation,[2,10,13] for example. Polymer–clay hybrid nanocomposite materials have recently attracted great research attention because the dispersing of nanolayered clay, in the form of intercalation or exfoliation, into various polymer matrices was found to boost the thermal stability,[1,2,4] mechanical strength,[8,9,10] gas barrier,[1,4,5] flame resistance,[14] and corrosion protection[1,5,7, 15,16] properties of bulk polymers. The earlier historical study of polymer–clay nanocomposite can be traced back to the work of polyamide–clay nanocomposites reported by Toyota's research group in 1990.[17]

Aromatic polyimides (PIs) are generally classified as thermally stable polymers that exhibit excellent mechanical strength and thermal stability among many engineering polymers. Research interests in aromatic PIs have increased in response to increasing high-technology applications in many fields (e.g., aerospace, automobile, and microelectronics). Recently, many synthetic efforts in the research field of high-temperature aromatic PIs have centered on promoting the processability and solubility of aromatic PIs through the synthesis of new diamine or dianhydride monomers. Several modifications to the PI backbone (e.g., introduction of flexible bridging linkages into the polymer backbone,[18,19] incorporation of bulky substituents along the polymer backbone[20,21]) have led to obvious success in the preparation of many soluble PIs. Currently, the literature continues to grow by numerous publications with respect to the preparation and properties of PI–clay nanocomposites[8,22–26] and soluble PI–clay nanocomposite materials.[27–29]

This article reports on a series of polymer–clay nanocomposite (PCN) materials, consisting of 4,4′-oxydianiline and 4,4′-(4,4′-isopropylidene-diphenoxy)-

Correspondence to: J.-M. Yeh (juiming@cycu.edu.tw).
Contract grant sponsor: National Science Council (NSC); contract grant number: 92-2113-M-033-011.

bis(phthalic anhydride) (ODA–BSAA) polyimide and layered montmorillonite (MMT) clay, that were successfully prepared by solution dispersion technique. The as-synthesized PCN materials were subsequently characterized by FTIR spectroscopy, wide-angle powder X-ray diffraction (XRD), transmission electron microscopy (TEM), and atomic force microscopy (AFM). Effects of the material composition on the anticorrosive performance, molecular permeability, and optical clarity of neat PI along with PCN materials, in the form of both coating and film, were studied by electrochemical corrosion measurement, molecular permeability analysis (GPA), and UV–visible transmission spectra, respectively.

EXPERIMENTAL

Chemicals and apparatus

4,4′-Oxydianiline (ODA; Fluka, Buchs, Switzerland), 1-methyl-2-pyrrolidone (NMP, 99.7%; Tedia, Fairfield, OH), *N,N*-dimethylacetamide (DMAc; (Mallinckrodt/Baker, Paris, KY), hexadecyltrimethylammonium chloride $[CH_3(CH_2)_{15}N(CH_3)_3^+Cl^-$, 99.9%, Acros Organics, Morris Plains, NJ], and 4,4′-(4,4′-isopropylidene diphenoxy)-bis(phthalic anhydride) (BSAA, 97%, Aldrich, Milwaukee, WI) were used as received without further purification. Montmorillonite (MMT) clay, having a cation-exchange capacity (CEC) value of 98 mequiv/100 g and a unit cell formula $Na^+_{0.31}$-$[Al_{1.67}Mg_{0.33}]Si_4O_{10}(OH)_2 \cdot 5.8H_2O$, was purchased from Pai-Kong Ceramic Co. (Taiwan). Electrochemical measurements of sample-coated cold-rolled steel (CRS) coupons were performed on a VoltaLab 21 and VoltaLab 40 potentiostat/galvanostat (Radiometer Analytical/London Scientific, Ontario, Canada) in a standard corrosion cell equipped with two graphite-rod counterelectrodes and a saturated calomel electrode (SCE) as well as the working electrode. FTIR spectra were recorded on pressed KBr pellets using an FTS-7 FTIR spectrometer (Bio-Rad, Hercules, CA). Wide-angle X-ray diffraction study of the samples was performed on a D/MAX-3C OD-2988N X-ray diffractometer (Rigaku, Tokyo, Japan) with copper target and Ni filter at a scanning rate of 4°/min. The samples for TEM study were first prepared by filling epoxy resin capsules with the powder of PCN materials followed by curing the epoxy resin at 100°C for 24 h in a vacuum oven. Then the cured epoxy resins, containing PCN materials, were microtomed with an Ultracut-E apparatus (Reichert-Jung GmbH, Arnsberg, Germany) into 60- to 90-nm thick slices. Subsequently, one layer of carbon, about 10 nm thick, was deposited on these slices on 100-mesh copper nets for TEM observations on a JEOL-200FX (JEOL, Tokyo, Japan) with an acceleration voltage of 120 kV. A model GTR 10 gas permeability analyzer (Yanagimoto Co., Kyoto, Japan) was used to carry out the permeation experiment of oxygen gas and water vapor. UV–visible transmission spectra were obtained using a U-2000 UV–visible spectrometer (Hitachi, Osaka, Japan). Atomic force microscopy (model DI 5000 AFM; Digital Instruments, Santa Barbara, CA) was used to probe the surface morphology of the coated films.

Synthesis of soluble polyimide derived from ODA–BSAA

A one-step method was used in this study. A typical procedure to prepare the polyimide (PI) is given as follows: BSAA (13.0 g, 0.025 mol) was added to 54.0 g of DMAc (denoted beaker A) at room temperature, with continuous stirring, for 30 min. A separate solution containing ODA (5.0 g, 0.025 mol) in another 30.0 g of DMAc (denoted beaker B) was prepared under mechanical stirring. After stirring for 30 min, the solution of beaker A was subsequently poured into the solution of beaker B. The as-prepared mixture was then stirred for an additional 48 h at 165°C under nitrogen gas purge. It was subsequently cooled to room temperature and poured onto the glass plate to form a white solid slice, followed by dipping in warm water, and subsequently dried under vacuum at 160°C for 12 h. The organo-soluble PI (13.8 g) was obtained in an approximately 77% yield.

Preparation of organophilic clay[1,4,5,7,15,16]

The organophilic clay was prepared by a cationic-exchange reaction between the sodium cations of MMT clay and quaternary alkylammonium cations $[CH_3(CH_2)_{15}N^+(CH_3)_3Cl^-]$ of the intercalating agent. The equation for calculating the intercalating agent used for a cationic-exchange reaction is expressed as follows:

$$98/100 \times 5 \text{ g (for clay)} \times 1.2 = (X/\text{MW of intercalating agent}) \times 1 \times 1000 \quad (1)$$

where 98/100 represents the CEC value per 100 g of MMT clay; 1.2 (>1) indicates the excess amount of intercalating agent used; and *X* and MW represent the amount and molecular weight of intercalating agent, respectively. Typically, 5 g of MMT clay, with a CEC value of 98 mequiv/100 g, was stirred in 400 mL of distilled water (beaker A) overnight at room temperature. A separate solution containing an excess amount of intercalating agent (2.5 g) in another 30 mL of distilled water (beaker B) was magnetically stirred, followed by the addition of 1*M* HCl aqueous solution to adjust the pH value to about 3–4. After the solution was stirred for 1 h, the protonated amino acid solution (beaker B) was added at a rate of about 10 mL/min,

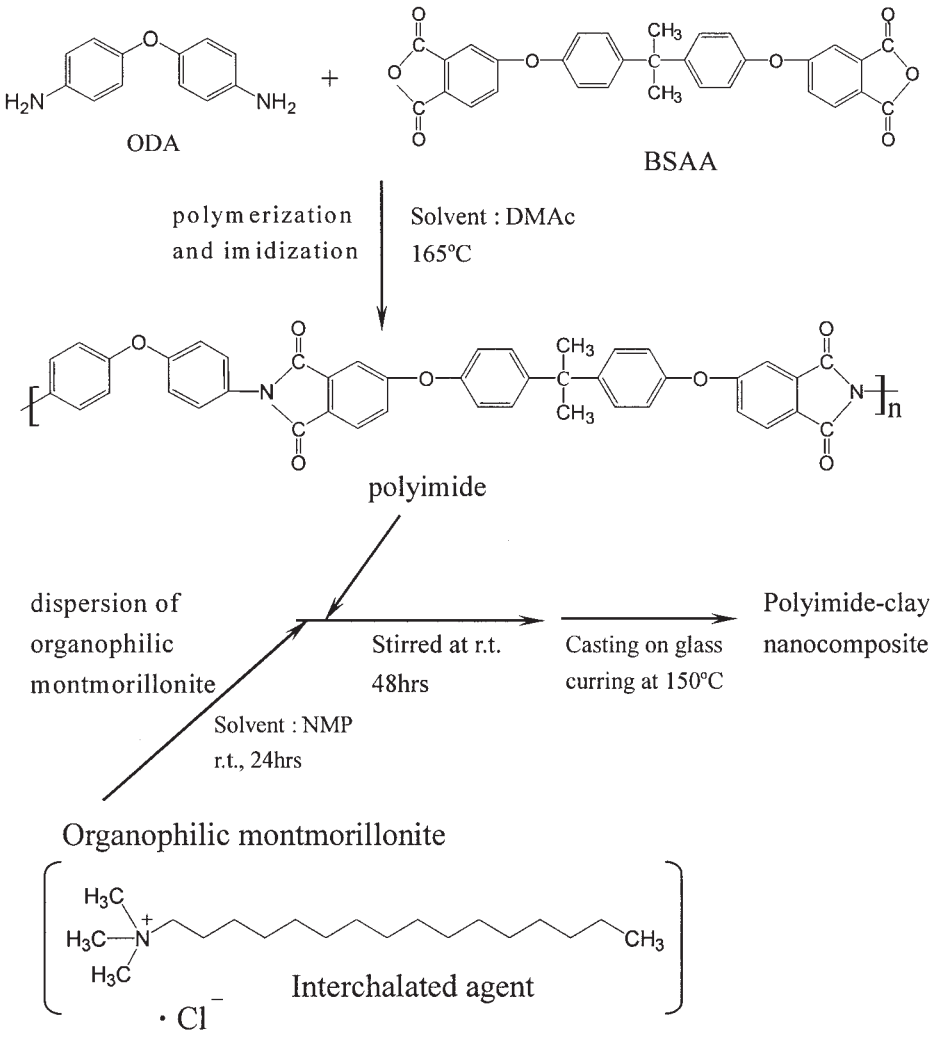

Scheme 1

with vigorous stirring, to the MMT suspension (beaker A). The mixture was stirred overnight at room temperature. The organophilic clay was recovered by ultracentrifugating (9000 rpm, 30 min) and filtering the solution in a Buchner funnel. Washing and filtering of samples were repeated at least three times to remove any excess ammonium ions accrued during purification of products.

Preparation of polyimide–clay nanocomposites (PCN)

A representative procedure of preparing the 3 wt % clay of PCN is given as follows: organophilic clay (0.0063 g) was introduced into 3.29 mL of NMP under magnetic stirring for 24 h at room temperature, after which 0.2037 g of PI was added to the solution and stirred for 48 h at room temperature. The solids content of solution was about 6 wt %.

Preparation of coatings and electrochemical measurements

The PCN solution was cast dropwise onto the CRS coupons (1.0 × 1.0 cm) followed by drying in air for 24 h at 40°C to give coatings of about 85 μm in thickness, measured by a digimatic micrometer (Mitutoyo, Tokyo, Japan). The coating ability of PCN solution on CRS is similar to that of bulk PI. The coated and uncoated coupons were then mounted on the working electrode so that only the coated side of the coupon was in direct contact with the electrolyte. The edges of the coupons were sealed with superfast epoxy cement. All the electrochemical measurements of corrosion potential, polarization resistance, and corrosion current were performed on a VoltaLab model 21 potentiostat/galvanostat and repeated at least three times. The electrolyte was an aqueous solution of NaCl (5 wt %). The open circuit potential at the equilibrium state of the system was recorded as the corrosion potential

(E_{corr} in V versus SEC). The polarization resistance (R_p in Ω/cm^2) was measured by sweeping the applied potential from 20 mV below to 20 mV about the E_{corr} at a scan rate of 500 mV/min and by recording the corresponding current change. The R_p value was obtained from the slope of the potential–current plot. The Tafel plots were obtained by the scanning potential from 250 mV below to 250 mV above the E_{corr} at a scan rate of 500 mV/min. The corrosion current (i_{corr}) was determined through superimposing a straight line along the linear portion of the cathodic or anodic curve and extrapolating it through E_{corr}. The corrosion rate (R_{corr}, in milli-inches per year, MPY) was calculated from the following equation:

$$R_{corr} = [0.13 \times i_{corr} \times (EW)]/[A \times d] \quad (2)$$

where EW is the equivalent weight (in g/equiv) of the CRS, A is the area (in cm^2) of the coated CRS, and d is the density (in g/cm^3) of the CRS. A VoltaLab model 40 potentiostat/galvanstat was used to perform the impedance spectroscopy studies. Impedance measurements were carried out in the frequency range 100 kHz to 100 mHz. The working electrode was first maintained in the test environment for 30 min to reach an equilibrium state before the impedance run. This served to put the electrode in a reproducible initial state and to make sure that no blistering occurred during the conditioning period. All experiments were performed at a room temperature of 25 ± 1°C. All data were replicated at least three times to ensure reproducibility and statistical significance.

Preparation of films and barrier property measurements

Typically, 3 mL of 3 wt % clay of PCN solution was cast onto a substrate (e.g., a microscope glass slide). The NMP solvent was allowed to evaporate at 150°C in an oven for 2 h. The sample-coated glass substrate was then immersed in distilled water at 70°C for 2 h to give the film of PCN materials. Oxygen permeabilities of the free-standing film were determined by using a GTR-10 gas permeability analyzer (Yanco Industries, Leeton, NSW, Australia). The gas permeability was measured by the following equation:

$$P = l/(p_1 - p_2) \times [(q/t)/A] \quad (3)$$

where P is the gas permeability [cm^3(STP) $(cm/cm^2)^{-1}$ s^{-1} $cmHg^{-1}$]; q/t is the volumetric flow rate of the gas permeate [cm^3(STP) s^{-1}]; l is the free-standing film thickness (cm); A is the effective free-standing film area (cm^2); and p_1 and p_2 are the pressures (cmHg) on the high-pressure and low-pressure sides of the free-standing film, respectively. The rate of transmission of O_2 was obtained by gas chromatography from which the air permeability was calculated. The experiment of water vapor permeation for membrane was performed according to our previously published report.[1] The feed solution was vaporized first and subsequently permeated through the membrane with an effective area of about 10.2 cm^2. The permeation rate was determined by measuring permeate weight.

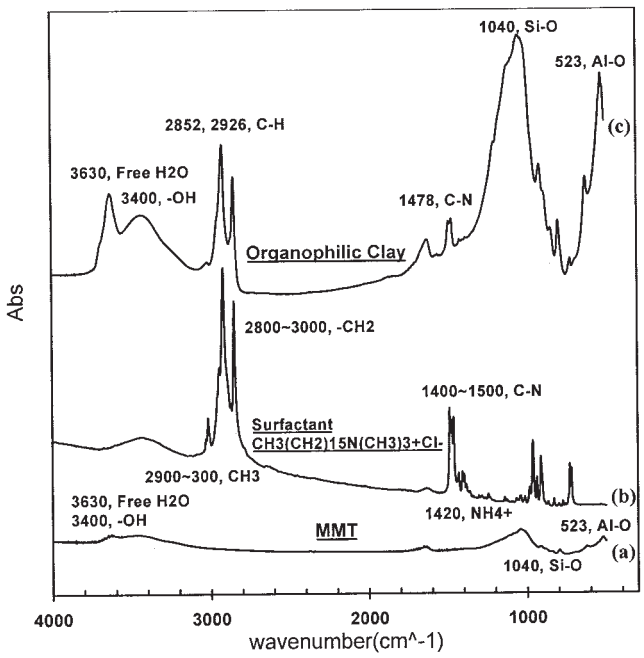

Figure 1 FTIR spectra of (a) clay (MMT), (b) intercalating agent, and (c) organophilic clay.

RESULTS AND DISCUSSION

For applications in coating studies, the flexible chemical structure was designed into the polyimide (PI) backbone to improve the solubility of PI in common organic solvents. The preparation flowchart of the soluble PI and PCN materials is shown in Scheme 1.

Characterization

The representative FTIR spectra of organophilic clay, intercalating agent, and montmorillonite (MMT) clay are shown in Figure 1. The characteristic vibration bands of MMT clay are found at 523 cm^{-1} (Al—O) and 1040 cm^{-1} (Si—O),[4,5,7,15,16] as shown in Figure 1(a). The vibration peaks of surfactant used as intercalating agent appeared at about 1420 cm^{-1} (NH_4^+), 950–1000 cm^{-1} (C—N), and 2900–3000 cm^{-1} (aliphatic hydrocarbons, $-CH_2-$), as shown in Figure 1(b). Furthermore, the characteristic bands of organophilic clay are shown in Figure 1(c). Figure 2 shows the FTIR spectra of neat PI and a series of PI–clay nanocomposite materials. As the loading of MMT clay is increased, the

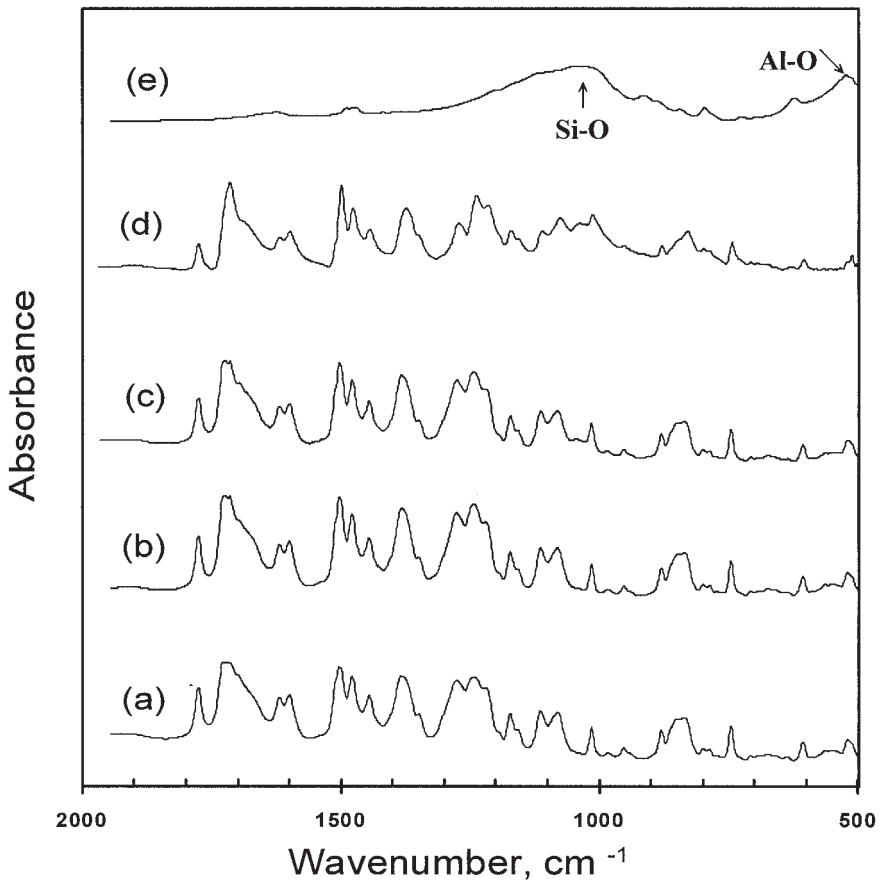

Figure 2 FTIR spectra of (a) PI, (b) CLPI3, (c) CLPI5, (d) CLPI10, and (e) organophilic clay.

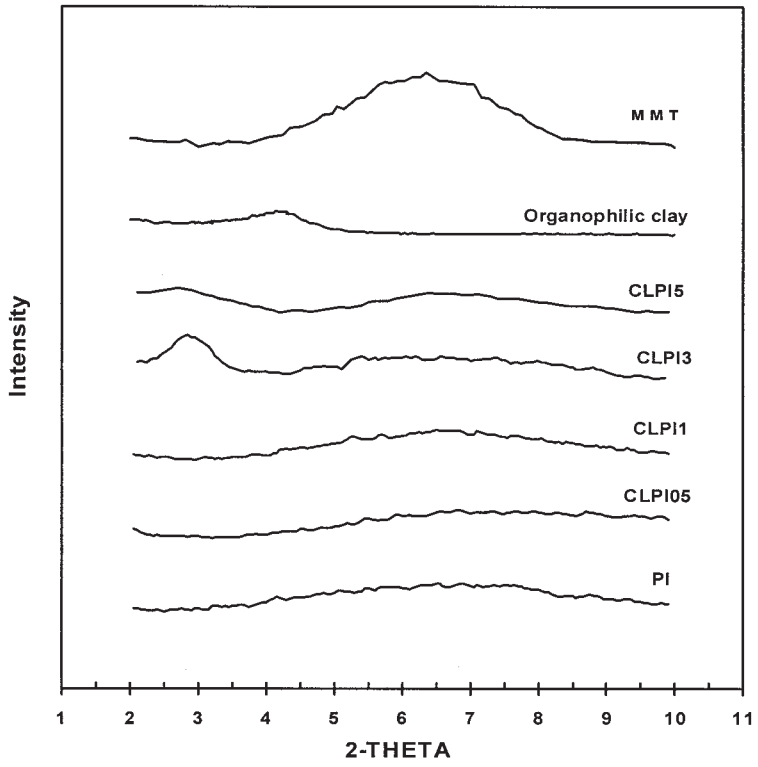

Figure 3 Wide-angle powder X-ray diffraction patterns of organophilic clay, PI, and a series of PI–clay nanocomposite materials.

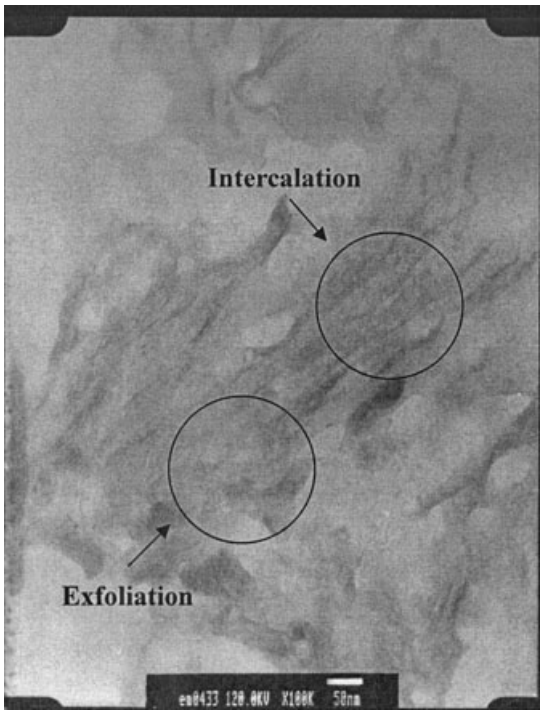

Figure 4 TEM micrograph of CLPI3 at ×100,000 magnification.

intensities of MMT clay bands become more pronounced. Figure 3 shows the wide-angle powder X-ray diffraction patterns of PI, MMT, organophilic clay, and a series of nanocomposite materials. There are no diffraction peaks for CLPI1 and CLPI05 in $2\theta = 2$–$10°$, as opposed to the diffraction peak at $2\theta = 4.3°$ (d-spacing = 2.05 nm) for organophilic clay, indicating the possibility of having exfoliated silicate nanolayers of organophilic clay dispersed in the PI matrix. When the amount of organophilic clay was increased to 3 wt %, there was a small peak appearing at $2\theta = 2.8°$ (d-spacing = 3.15 nm), implying that there is a small amount of organophilic clay that cannot exfoliate in the PI existing in the form of an intercalated layer structure. In Figure 4, the TEM micrograph of PI–clay material, with 3 wt % clay loading, shows that the nanocomposite has a combinational morphology, simultaneously including both exfoliated and intercalated nanolayer structures in the polymer matrix.

AFM studies of nanocomposite morphology

To further gain the physical fundamentals of the topographical structures in more detail, AFM was applied to investigate the surface profiles of the samples, as shown in Figure 5, which exhibit a 3D topographical feature of the neat PI and CLPI3. By roughness analysis, we found that the mean roughness (Ra in nm) of CLPI3 is 5.097, which is larger than that of neat PI ($Ra = 2.269$ nm). Both the 3D image and the roughness analysis demonstrate a slight smooth decrease as the PI matrix incorporated with 3 wt % loading of organophilic clay.

Anticorrosive performance of nanocomposite coatings

The anticorrosive performance of sample-coated CRS coupons was evaluated based on the corrosion potential (E_{corr}), polarization resistance (R_p), corrosion current (i_{corr}), and corrosion rate (R_{corr}), as listed in Table I. The CRS coupon coated with PI shows a higher E_{corr} value than that of the uncoated CRS, although it exhibits a lower E_{corr} value than that of the specimen coated with PCN materials. For example, the CLPI05-

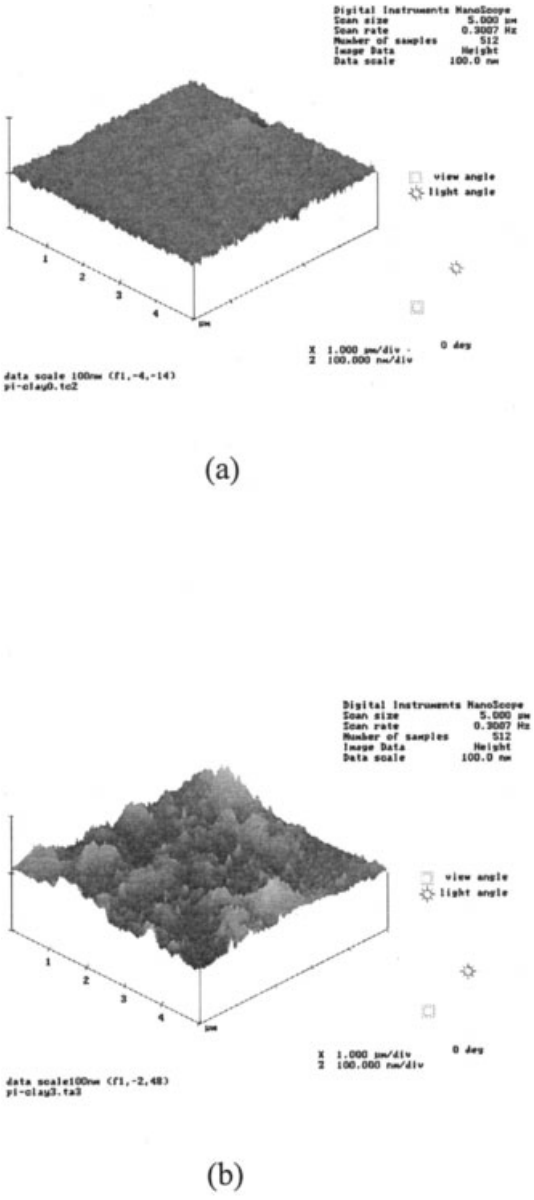

Figure 5 Atomic force microscopy (AFM) studies of (a) PI and (b) CLPI3.

TABLE I
Relationships of the Composition of Polyimide (PI)–MMT Clay Nanocomposite Materials with the E_{corr}, R_p, i_{corr}, and R_{corr} Measured from Electrochemical Methods[a]

Compound code	Feed composition (wt %)		Inorganic content found in product[b] (wt %)	Electrochemical corrosion measurements			
	Polyimide	MMT		E_{corr} (mv)	R_p (kΩ/cm^2)	i_{corr} (μA/cm^2)	R_{corr} (MPY)
Bare				−687.1	9.33	5.0943	2.2924
PI	100	0	44.82	−588.7	95.6	0.758	0.3411
CLPI05	99.5	0.5	44.87	−547.4	117.5	0.3195	0.1438
CLPI1	99	1	44.56	−506.9	610.9	0.0907	0.0408
CLPI3	97	3	44.77	−484.4	1150	0.0579	0.0261
CLPI5	95	5	42.62	−306.8	2450	0.0246	0.0111

[a] Saturated calomel electrode was used as reference electrode.
[b] As determined TGA measurements at 800°C.

coated CRS has a high corrosion potential of about −547.4 mV at 30 min. Even after a 5-h measurement, the potential remains at about −550 mV. Such an E_{corr} value implies that the CLPI05-coated CRS is much noble toward the electrochemical corrosion compared to the PI. The CLPI05-coated CRS shows a polarization resistance (R_p) value of 117.5 kΩ/cm^2 in 5 wt % NaCl, which approaches 2 orders of magnitude greater than that of the uncoated CRS. The Tafel plots for (a) uncoated, (b) PI-coated, (c) CLPI3-coated, and (d) CLPI5-coated CRS are shown in Figure 6. For example, the i_{corr} value of CLPI05-coated CRS is about 0.3195 μA/cm^2, which corresponds to an R_{corr} value of about 0.1438 milli-inches per year (MPY) (Table I). Electrochemical impedance spectroscopy (EIS) was also used to examine the activity difference between CRS surfaces after PI and PCN material treatment. Four samples were prepared at this evaluation. The first sample (a) was PI-coated CRS. A series of samples, denoted by (b)–(d), were coated by PCN materials with different clay loadings. EIS evaluations were performed in 5 wt % aqueous NaCl electrolyte for 30 min. Figure 7 shows the Nyquist plots of the four samples. Charge transfer resistances of samples (a)–(d), as determined by the intersection of the low-frequency end of the semicircle arc with the real axis, are 2.25, 2.75, 6.45, and 8.40 MΩ cm^{-2}), respectively. Results clearly demonstrate that the sample, with the high clay loading up to 5 wt %, has the greatest anticorrosion performance. Electrochemical corrosion current values of PCN materials as coatings on CRS were found to decrease gradually with further increases in clay loading. This novel

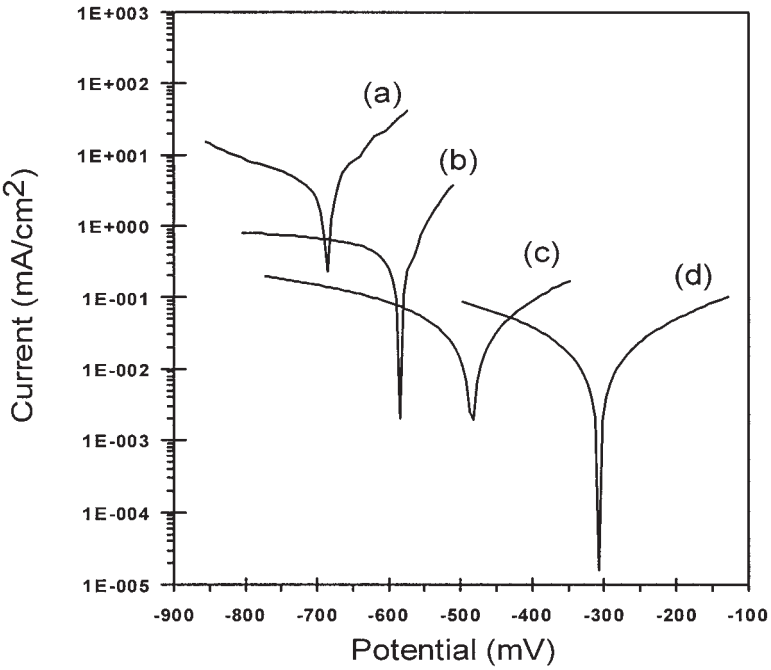

Figure 6 Tafel plots for (a) uncoated, (b) PI-coated, (c) CLPI3-coated, and (d) CLPI5-coated CRS coupons measured in 5 wt % NaCl aqueous solution.

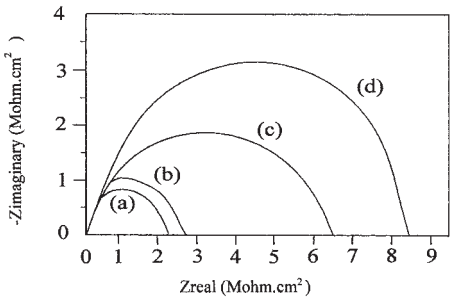

Figure 7 Nyquist plots of four sample-coated CRS coupons measured in 5 wt % NaCl aqueous solution: (a) PI-coated, (b) CLPI05-coated, (c) CLPI3-coated, (d) CLPI5-coated.

property of enhanced anticorrosion effect for PI–clay nanocomposite materials, compared to that of bulk PI, may be attributed to dispersing silicate nanolayers of clay in the PI matrix to increase the tortuosity of diffusion pathways of oxygen and water.[1,5] This is further evidenced by the studies of the effect of O_2 and H_2O molecular barriers, as discussed in the following section.

Molecular barrier properties of nanocomposite films

In this study, free-standing films of PCN materials and bulk PI, used for the molecular barrier measurements, were prepared with a film thickness of about 30 μm. Compared to PI, free-standing film of PCN materials at low clay loading (e.g., 0.5 wt %) shows about 48 and 46% decrease in H_2O and O_2 permeability, respectively, as shown in Figure 8. Furthermore, it should be noted that a further increase of clay loading results in a slightly further enhanced molecular barrier property of bulk PCN materials. However, free-standing film of PCN at high clay loading (e.g., 5 wt %) shows larger O_2/H_2O permeability. This may be associated with the phase separation resulting from the nanocomposite at high clay loading.[15]

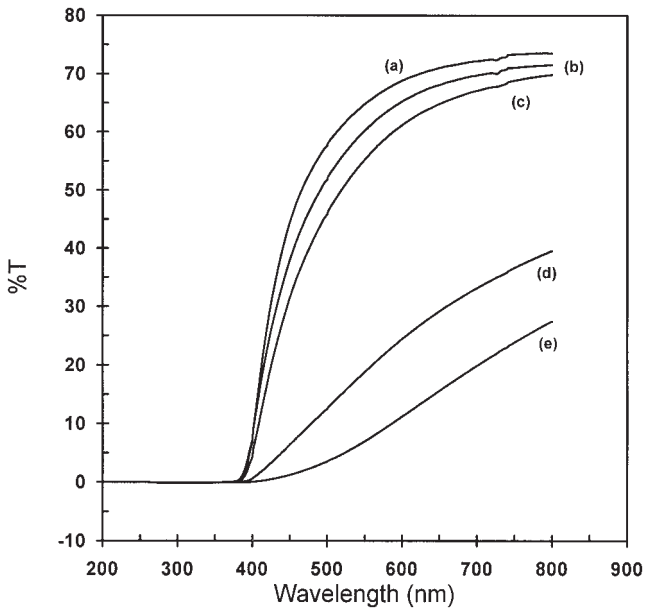

Figure 9 UV–visible transmission spectra of nanocomposite free-standing films of (a) PI, (b) CLPI5, (c) CLPI1, (d) CLPI3, and (e) CLPI5.

Optical clarity of nanocomposite film

Figure 9(a)–(c) show the UV–vis transmission spectra of pure PI and PCNs with 0.5 and 1 wt % MMT. These

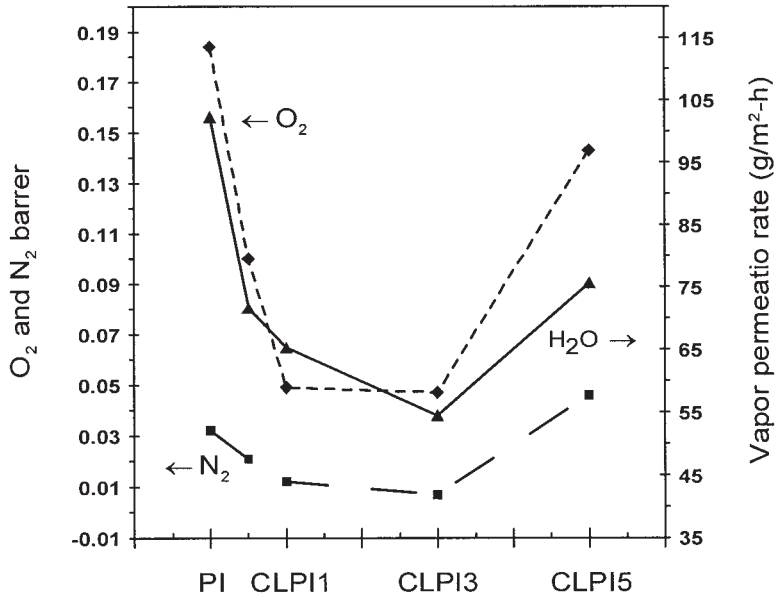

Figure 8 Permeability of H_2O and O_2 as a function of the MMT clay content in the PI–clay nanocomposite materials.

membranes have a thickness of about 40 μm. The spectra of CLPI1 show that the visible region (400–700 nm) is slightly affected by the presence of the clay, retaining the high transparency of the PI and indicating the primarily exfoliated composites.[1] Furthermore, CLPI3 has a much lower transparency than that of either CLPI0.5 or CLPI1, and very close to that of CLPI5. This result suggests that PCN3 may have a mixed morphology like that of CLPI5. A close look at XRD patterns (Fig. 3) suggests a broad peak around 5°, which is also evidence for the mixed morphology. However, the spectra of CLPI5, exhibiting low transparency of the PI, reflect the primarily intercalated composites.[1] For the ultraviolet wavelength, there is strong scattering and/or absorption, leading to a lower transmission of the UV light.[1]

CONCLUSIONS

This article reports on a series of polymer–clay nanocomposite materials, consisting of organo-soluble polyimide (ODA-BSAA) matrix and dispersed nanolayers of inorganic montmorillonite clay, prepared by a solution dispersion technique and subsequently characterized by FTIR, powder X-ray diffraction patterns, transmission electron microscopy, and atomic force microscopy.

Effects of the materials composition on the corrosion protection performance, gas barrier, and optical properties, in the form of both coating and free-standing film, were also studied by electrochemical corrosion measurements, gas permeability analysis, and UV–visible transmission spectroscopy, respectively. Compared to neat PI, PCN coatings show enhanced corrosion protection effect on cold rolled steel coupons based on the electrochemical corrosion potential, polarization resistance, corrosion current, and impedance spectroscopy studies. PCN free-standing films are also found to exhibit enhanced O_2/H_2O gas barrier properties, compared to those of the neat PI film, based on the gas permeability studies. The optical clarity of PCN films is found to display high transparency and low transparency at low clay and high clay loading, respectively, based on the UV–visible transmission spectroscopy studies.

The authors gratefully acknowledge the financial support of this research by the National Science Council (Grant 92-2113-M-033-011).

References

1. Yeh, J.-M.; Liou, S.-J.; Lin, C.-Y.; Cheng, C.-Y.; Chang, Y. W.; Lee, K. R. Chem Mater 2002, 14, 154.
2. Sikka, M.; Cerini, L. N.; Ghosh, S. S.; Winey, K. I. J Polym Sci Part B: Polym Phys 1996, 34, 1443.
3. Seckin, T.; Gultek, A.; Lcduygu, M. G.; Onal, Y. J Appl Polym Sci 2002, 84, 164.
4. (a) Yeh, J.-M.; Yu, M.-Y.; Liou, S.-J. J Appl Polym Sci 2003, 89, 3632; (b) Yu, Y.-H.; Lin, C.-Y.; Yeh, J.-M.; Lin, W.-H. Polymer 2003, 44, 3553.
5. Yeh, J.-M.; Liou, S.-J.; Lai, C.-Y.; Wu, P.-C.; Tsai, T.-Y. Chem Mater 2001, 13, 1131.
6. Oriakhi, C. O.; Lerner, M. M. Mater Res Bull 1995, 30, 723.
7. Yeh, J.-M.; Chin, C.-P.; Chang, S. J Appl Polym Sci 2003, 88, 3264.
8. Tyan, H.-L.; Liu, Y.-C.; Wei, K.-H. Chem Mater 1999, 11, 1942.
9. Park, S. J; Seo, D. I.; Lee, J. R. J Colloid Interface Sci 2002, 251, 160.
10. Cho, J. W.; Paul, D. R. Polymer 2001, 42, 1083.
11. Huang, X.; Brittain, W. J. Macromolecules 2001, 34, 3255.
12. Muzrny, C. D.; Butler, B. D.; Hanley, H. J. M.; Tsvetkov, F.; Peiffer, D. G. Mater Lett 1996, 28, 379.
13. Limary, R.; Swinnea, S.; Green, P. F. Macromolecules 2000, 33, 5227.
14. Gilman, J. W.; Jackson, C. L.; Morgan, A. B.; Harris, R. H.; Manias, E.; Giannelis, E. P.; Wuthenow, M.; Hilton, D.; Phillips, S. Chem Mater 2000, 12, 1866.
15. Yeh, J.-M.; Chen, C.-L.; Chen, Y.-C.; Ma, C.-Y.; Lee, K.-R.; Wei, Y.; Li, S. Polymer 2003, 43, 2729.
16. Yeh, J. M.; Chin, C.-P. J Appl Polym Sci 2003, 88, 1072.
17. Usuki, A.; Kawasumi, M.; Kojima, Y.; Okada, A.; Karauchi, T.; Kamigaito, O. J Mater Res. 1993, 8, 1774.
18. Feld, W. A.; Ramalingam, B.; Harris, F. W. J Polym Sci Polym Chem Ed 1983, 21, 319.
19. Imai, Y.; Maldar, N. N.; Kakimoto, M. J Polym Sci Part A: Polym Chem 1984, 22, 2189.
20. Giesa, R.; Keller, U.; Schmidt, H. W. ACS Polym Prepr 1992, 33, 396.
21. Jadhav, T. Y.; Preston, J; Krigbaum, W. R. J Polym Sci Part A: Polym Chem 1989, 27, 1175.
22. Morgan, A. B.; Gilman, J. W.; Jackson, C. L. Macromolecules 2001, 34, 2735.
23. Agag, T.; Koga, T.; Takeichi, T. Polymer 2001, 42, 3399.
24. Gu, A.; Kuo, S.-W.; Chang, F.-C. J Appl Polym Sci 2001, 79, 1902.
25. Huang, J.-C.; Zhu, Z. K.; Yin, J.; Qian, X. F.; Sun, Y.-Y. Polymer 2001, 42, 873.
26. Gu, A.; Chang, F.-C. J Appl Polym Sci 2001, 79, 289.
27. Zhu, Z. K.; Yang, Y.; Yin, J.; Wang, X.-Y.; Ke, Y.-C.; Qi, Z.-N. J Appl Polym Sci 1999, 73, 2063.
28. Hsiao, S.-H.; Liou, G.-S.; Chang, L.-M. J Appl Polym Sci 2001, 80, 2067.
29. Huang, J.-C.; Zhu, Z.-K.; Ma, X.-D.; Qian, X.-F.; Yin, J. J Mater Sci 2001, 36, 871.